Published in final edited form as:
Angew Chem Int Ed Engl. 2014 March 3; 53(10): 2735–2738. doi:10.1002/anie.201310841.

Fourier Transform EPR Spectroscopy of Trityl Radicals for Multifunctional Assessment of Chemical Microenvironment**

Dr. Andrey A. Bobko,
Dorothy M. Davis Heart & Lung Research Institute and Division of Pulmonary, Allergy Critical Care & Sleep Medicine, Department of Internal Medicine, The Ohio State University, 201 HLRI, 473 W 12th Ave, Columbus, OH 43210 (USA)

Dr. Ilirian Dhimitruka,
Dorothy M. Davis Heart & Lung Research Institute and Division of Pulmonary, Allergy Critical Care & Sleep Medicine, Department of Internal Medicine, The Ohio State University, 201 HLRI, 473 W 12th Ave, Columbus, OH 43210 (USA)

Prof. Dr. Jay L. Zweier, and
Dorothy M. Davis Heart & Lung Research Institute and Division of Cardiovascular Medicine, Department of Internal Medicine, The Ohio State University, Ohio (USA)

Prof. Dr. Valery V. Khramtsov
Dorothy M. Davis Heart & Lung Research Institute and Division of Pulmonary, Allergy Critical Care & Sleep Medicine, Department of Internal Medicine, The Ohio State University, 201 HLRI, 473 W 12th Ave, Columbus, OH 43210 (USA)

Valery V. Khramtsov: Valery.Khramtsov@osumc.edu

Abstract

Pulse techniques in electron paramagnetic resonance (EPR) allow for a reduction in measurement times and increase in sensitivity but require the synthesis of paramagnetic probes with long relaxation times. Here it is shown that the recently synthesized phosphonated trityl radical possesses long relaxation times that are sensitive to probe the microenvironment, such as oxygenation and acidity of an aqueous solution. In principle, application of Fourier transform EPR (FT-EPR) spectroscopy makes it possible to acquire the entire EPR spectrum of the trityl probe and assess these microenvironmental parameters within a few microseconds. The performed analysis of the FT-EPR spectra takes into consideration oxygen-, proton-, buffer-, and concentration-induced contributions to the spectral shape, therefore enabling quantitative and discriminative assessment of pH, pO_2, and concentrations of the probe and inorganic phosphate.

Keywords

biosensors; EPR spectroscopy; relaxation times; radicals

Pulsed electron paramagnetic resonance (EPR) spectroscopy is currently undergoing rapid developments based on the advances in radiofrequency (RF) electronics and synthesis of the probes with comparatively long relaxation times.[1–7] Recently we synthesized dual function

**Financial support from NIH grant numbers EB014542, EB016859, and EB016096 is acknowledged.

Correspondence to: Valery V. Khramtsov, Valery.Khramtsov@osumc.edu.

Supporting information for this article is available on the WWW under http://dx.doi.org/10.1002/anie.201310841.

oxygen- and pH-sensitive phosphonated trityl probes and demonstrated their application in vitro and in vivo for concurrent assessment of pO_2 and pH using continuous-wave (CW) EPR spectroscopy.[8] In principle, long relaxation times of the trityl probes allow extending these functional measurements using FT-EPR techniques. In contrast to applied FT-NMR spectroscopy, and in spite of the principal advantages in high sensitivity and low detection time, FT-EPR spectroscopy has been rarely used in studies of aqueous solutions because of the lack of suitable functional probes.

Table 1 lists the values of longitudinal, T_1, and transverse, T_2, relaxation times of the p_1TAM probe measured in aqueous solutions of different pH values that correspond to different ionization states of the phosphono group (see Scheme 1) in ambient air or under anoxic conditions. The values measured under anoxic conditions are in a good agreement with the previously reported data for symmetrical deuterated Finland trityl (T_1 = 17 μs, T_2 = 11 μs).[5]

Long relaxation times of p_1TAM allow for excitation of the whole EPR spectrum using a 20 ns π/2 pulse followed by detection of the free induction decay (FID; Figure 1a). Figure 1b shows the absorption EPR spectrum obtained by Fourier transformation (FT) of the time-domain FID signal. The FT-EPR spectrum represents a superposition of two ionization states of the probe, A (p_1TAM^{3-}) and B (p_1TAM^{4-}) with protonated and unprotonated phosphono groups, respectively (see Scheme 1), which have different phosphorus hyperfine constants, a_P(A) = 10191 kHz and a_P(B) = 9422 kHz, and different g-factors (Δg =90 kHz).

Figure 2 shows the high-frequency component of the FT-EPR spectra of p_1TAM solutions at different pH values and oxygen concentrations measured after application of selective 96 ns pulse. Figure 2 clearly demonstrates the independent character of pH and oxygen spectral sensitivities, signal intensity ratio (Figure 2a), and linewidth (Figure 2b). Accordingly, the simulation of the spectra yields the values of the probe fractions, p_A and p_B, and oxygen-induced relaxation rates, $R_{O2}{}^A$ and $R_{O2}{}^B$, for the forms A and B, respectively (see the Supporting Information). Figure 3a shows the dependence of the fraction p_A on the pH value which is described by a standard titration curve with $pK_a{}^2$ = 6.85 ± 0.05. Figure 3b shows the dependencies of $R_{O2}{}^A$ and $R_{O2}{}^B$ on the oxygen partial pressure that can be fitted by linear functions yielding the values of the corresponding bimolecular rate constants of the spin exchange between the trityl probe and oxygen, $k_{O2}{}^A$ =1.51 kHzmmHg^{-1} and $k_{O2}{}^B$ = 1.38 kHzmmHg^{-1}. Assuming an oxygen solubility in 150 mM NaCl aqueous solution at 22°C and pO_2 = 760 mmHg of about 1.28 mM, we obtain values of $k_{O2}{}^A$ ==0.9 × 10^9M^{-1}s^{-1} and $k_{O2}{}^B$ =0.82 × 10^9M^{-1}s^{-1} being close to the rate constants for diffusion-controlled reactions.

In general, three different types of exchange reactions may contribute to the FT-EPR spectra of the p_1TAM probe, namely spin exchange of p_1TAM with oxygen, spin self-exchange between trityl radicals, and proton exchange between different ionization states of p_1TAM. Fortunately, the manifestation of these reactions in the EPR spectra have distinguished features and can be quantitatively separated.

In contrast to oxygen-induced line broadening, proton exchange also results in narrowing the distance between the EPR lines that correspond to different ionization states but the same projections of the nuclear spin of phosphorus, namely, A (S_p = 1/2) and B (S_p = 1/2); and A (S_p = −1/2) and B (S_p = −1/2) (see Figure 1 and section 1 in the Supporting Information). The normalized rates (in Hz) of proton loss by the phosphono group of the p_1TAM^{3-} form, $R^A{}_{H+}$, and proton addition to the phosphono group of the p_1TAM^{4-} form, $R^B{}_{H+}$, in the reaction of p_1TAM with solvated protons at neutral pH are too low to affect the EPR spectrum because of the low proton concentrations. However, the proton exchange reactions

between radical and buffer molecules with the pK_a^B close to the pK_a^2 of p_1TAM may significantly enhance the rates R^A_{H+} and R^B_{H+}. Figure 4 shows FT-EPR spectra measured in deoxygenated saline solutions at low probe concentration but different concentrations of phosphate buffer (pK_a^B =6.66).[9] The observed spectral changes are characteristic for frequency exchange induced by a proton exchange reaction between phosphonated trityl groups and phosphate anions described by Equation (1).[8,10,11]

$$p_1TAM^{3-} + HPO_4^{2-} \underset{k_r}{\overset{k_f}{\rightleftarrows}} p_1TAM^{4-} + H_2PO_4^- \quad (1)$$

The ratio R^A_{H+}/R^B_{H+} is equal to the ratio of inverse lifetimes of the radical in the forms A and B or the fraction ratio, so $R^B_{H+} = R^A_{H+} \times p_A/(1-p_A)$. Figure 6a shows that the R^A_{H+} values obtained from spectra fittings are directly proportional to the phosphate buffer concentration. The linear approximation yields the value of the bimolecular rate constants, $k_f = 2.1 \times 10^7 M^{-1}s^{-1}$ and $k_r = 3.3 \times 10^7 M^{-1}s^{-1}$ (see the Supporting Information).

Spin self-exchange between trityl radicals in addition to line broadening results in a shift of the positions of all the EPR lines of p_1TAM (see Figure SI1 for the details). Figure 5 shows the effect of spin self-exchange between trityl radicals on the EPR spectra of p_1TAM measured in deoxygenated saline solutions in the absence of phosphate buffer but at different probe concentrations. The simulation of the spectra yields values of the observed rates of spin self-exchange, k_{AA}*, k_{BB}*, and k_{AB}* (in Hz), between p_1TAM in the ionization states p_1TAM^{3-}, p_1TAM^{4-} and between the radicals in different ionization states. Figure 6b shows the dependencies of the rates k_{AA}*, k_{BB}*, and k_{AB}*, on the p_1TAM concentration that allows for linear approximation yielding the value of the corresponding bimolecular rate constants of spin self-exchange, $k_{AA} = 1.43 \times 10^7 M^{-1}s^{-1}$, $k_{BB} = 0.74 \times 10^7 M^{-1}s^{-1}$, and $k_{AB} = 10^7 M^{-1}s^{-1}$.

The bimolecular rate constants were found to have values 1) about $10^9 M^{-1}s^{-1}$ for the spin exchange of p_1TAM with a small oxygen diradical molecule, 2) almost two orders of magnitude lower, in the range $(2.1–3.3) \times 10^7 M^{-1}s^{-1}$, for the proton exchange reactions of p_1TAM with phosphate anions, and 3) the lowest values, $(0.74–1.43) \times 10^7 M^{-1}s^{-1}$, for the spin self-exchange between large trityl radicals. This tendency is consistent with the significant contribution of steric hindrance in the reactivity of trityl radicals.

In the general case, analysis of the FT-EPR spectrum of p_1TAM allows for simultaneous extraction pH, pO_2, and the concentrations of inorganic phosphate, [Pi], and of the probe, [p_1TAM]. Table 2 lists the values of these four parameters calculated from the spectra (see Figure SI3) of various p_1TAM solutions that are in a good agreement with the sample compositions. An accuracy of determination of pO_2 is about 1 mmHg (or 1 mμ [O_2]) which is two orders of magnitude higher than that for concentrations of Pi or p_1TAM, about 0.1 mM. This is in agreement with an accuracy of spectral linewidth analysis of about 1 kHz, and the rate constant values for oxygen-induced spin exchange of about $10^9 M^{-1}s^{-1}$ and for proton exchange and spin self-exchange reactions of about $10^7 M^{-1}s^{-1}$.

In summary, FT-EPR spectroscopy using the p_1TAM probe makes possible the concurrent measurement of the four parameters of the probe microenvironment, namely pO_2, pH, [Pi], and [p_1TAM]. Taking into account a sufficient depth of low radiofrequency penetration into aqueous samples, this provides a new tool for simultaneous in vivo assessment of several tissue parameters that play important roles in physiology and pathophysiology of living organisms including: tissue oxygenation, acidosis, Pi concentrations, and perfusion (probe distribution).[12,13] Tissue pO_2 and extracellular pH are well-recognized hallmarks in solid

tumors while extracellular Pi has been recently identified as a new signaling molecule of importance in tumorigenesis.[14–16] Importantly, an extraordinary high sensitivity of p_1TAM to pO_2 allows to detect a oxygen tension as low as the threshold of anoxia, about 1 mmHg. p_1TAM possesses a pH sensitivity in a physiologically important pH range that makes it possible to monitor the acidity both in normal tissues and in acidic tumors. The range of Pi measured by pTAM from 0.1 to 20 mM covers the physiological range of the Pi values previously reported in the literature.[17,18] This unique multifunctional sensitivity of the p_1TAM probe decreases the method invasiveness and will allow for a better correlation of the parameters independent of the distribution of the probe. The demonstrated FT-EPR application can be extended to imaging modalities[19–21] taking into account the simple EPR spectrum and long relaxation times of the p_1TAM probe (Table 1).

Supplementary Material

Refer to Web version on PubMed Central for supplementary material.

References

1. Schweiger, A.; Jeschke, G. Principles of pulse electron paramagnetic resonance. Oxford University Press; Oxford, New York: 2001.
2. Murugesan R, Cook JA, Devasahayam N, Afeworki M, Subramanian S, Tschudin R, Larsen JA, Mitchell JB, Russo A, Krishna MC. Magn Reson Med. 1997; 38:409. [PubMed: 9339442]
3. Prisner T, Rohrer M, MacMillan F. Annu Rev Phys Chem. 2001; 52:279. [PubMed: 11326067]
4. Sicoli G, Wachowius F, Bennati M, Hobartner C. Angew Chem. 2010; 122:6588.Angew Chem Int Ed. 2010; 49:6443.
5. Yong L, Harbridge J, Quine RW, Rinard GA, Eaton SS, Eaton GR, Mailer C, Barth E, Halpern HJ. J Magn Reson. 2001; 152:156. [PubMed: 11531374]
6. Reginsson GW, Kunjir NC, Sigurdsson ST, Schiemann O. Chem Eur J. 2012; 18:13580. [PubMed: 22996284]
7. Yang Z, Liu Y, Borbat P, Zweier JL, Freed JH, Hubbell WL. J Am Chem Soc. 2012; 134:9950. [PubMed: 22676043]
8. Dhimitruka I, Bobko AA, Eubank TD, Komarov DA, Khramtsov VV. J Am Chem Soc. 2013; 135:5904. [PubMed: 23517077]
9. Butler, JN. Ionic equilibrium: solubility and pH calculations. Wiley; New York: 1998.
10. Bobko AA, Dhimitruka I, Komarov DA, Khramtsov VV. Anal Chem. 2012; 84:6054. [PubMed: 22703565]
11. Driesschaert B, Marchand V, LevÞque P, Gallez B, March-and-Brynaert J. Chem Commun. 2012; 48:4049.
12. Siemann, DW., editor. Tumor Microenvironment. Wiley; Chi-chester: 2011.
13. Bobko AA, Eubank TD, Voorhees JL, Efimova OV, Kirilyuk IA, Petryakov S, Trofimiov DG, Marsh CB, Zweier JL, Grigor'ev IA, Samouilov A, Khramtsov VV. Magn Reson Med. 2012; 67:1827. [PubMed: 22113626]
14. Chang SH, Yu KN, Lee YS, An GH, Beck GR Jr, Colburn NH, Lee KH, Cho MH. Am J Respir Cell Mol Biol. 2006; 35:528. [PubMed: 16763222]
15. Spina A, Sapio L, Esposito A, Di Maiolo F, Sorvillo L, Naviglio S. BioResources. 2013; 2:47.
16. Khoshniat S, Bourgine A, Julien M, Weiss P, Guicheux J, Beck L. Cell Mol Life Sci. 2011; 68:205. [PubMed: 20848155]
17. Stubbs M, Bhujwalla ZM, Tozer GM, Rodrigues LM, Maxwell RJ, Morgan R, Howe FA, Griffiths JR. NMR Biomed. 1992; 5:351. [PubMed: 1489671]
18. Fogh-Andersen N, Altura BM, Altura BT, Siggaard-Andersen O. Clin Chem. 1995; 41:1522. [PubMed: 7586528]
19. Epel B, Sundramoorthy SV, Mailer C, Halpern HJ. Concepts Magn Reson Part B. 2008; 33B:163.

20. Yasui H, Matsumoto S, Devasahayam N, Munasinghe JP, Choudhuri R, Saito K, Subramanian S, Mitchell JB, Krishna MC. Cancer Res. 2010; 70:6427. [PubMed: 20647318]

21. Blank A, Freed JH. Isr J Chem. 2006; 46:423.

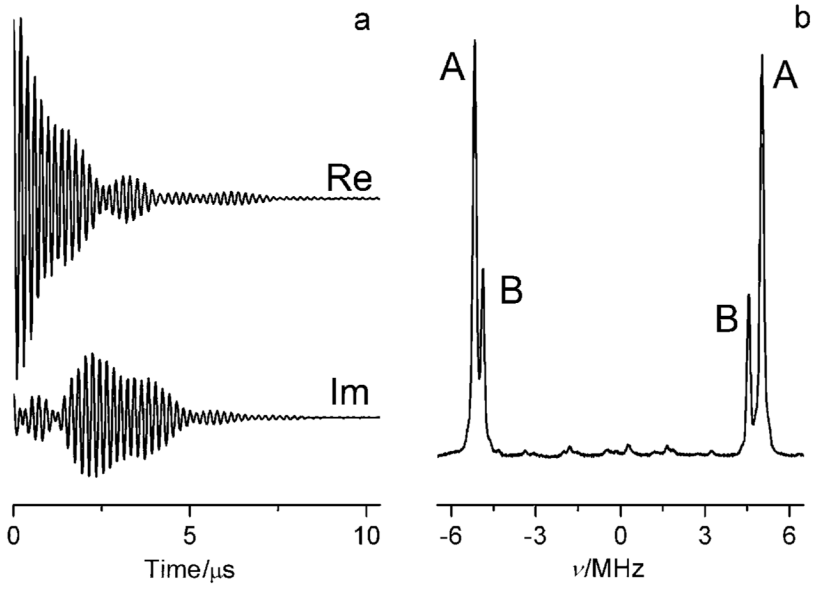

Figure 1.

Real (Re) and imaginary (Im) parts of the X-band EPR FID signal of 0.2 mM p_1TAM solution, pH 6.4, measured a) after applying a nonselective 20 ns π/2 pulse and b) the corresponding FT-EPR spectrum. The EPR spectral lines correspond to the four trityl radical states: A ($S_p = -1/2$), B ($S_p = -1/2$), B ($S_p = 1/2$), and A ($S_p = 1/2$).

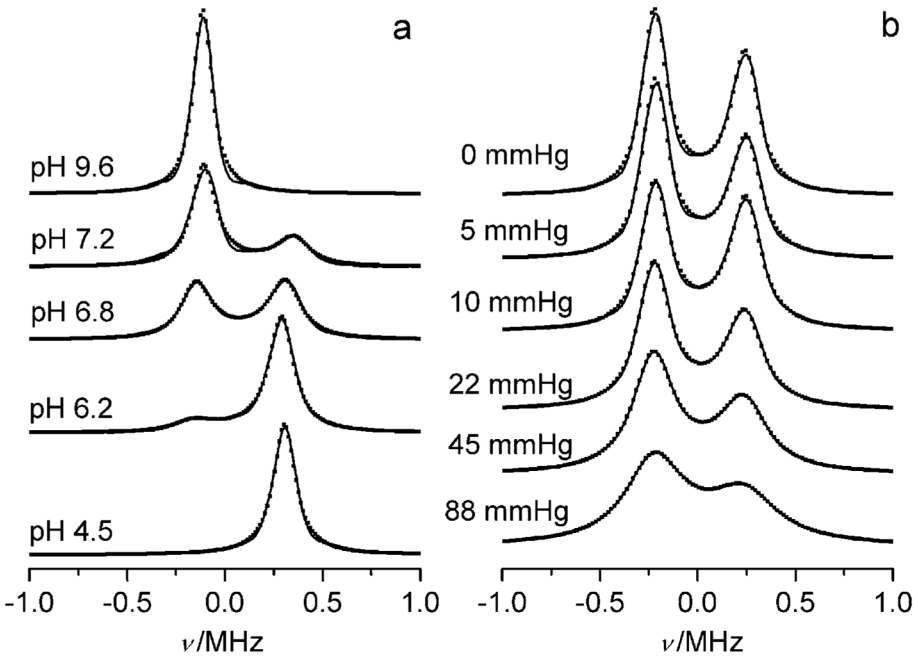

Figure 2.

High-frequency component of the FT-EPR spectra of 0.2 mM p_1TAM in 150 mM aqueous NaCl solutions a) at different pH values and b) under different oxygen partial pressures in the presence of a a) 2 mM or b) 0.5 mM Na-phosphate buffer. The dotted lines are calculated spectra.

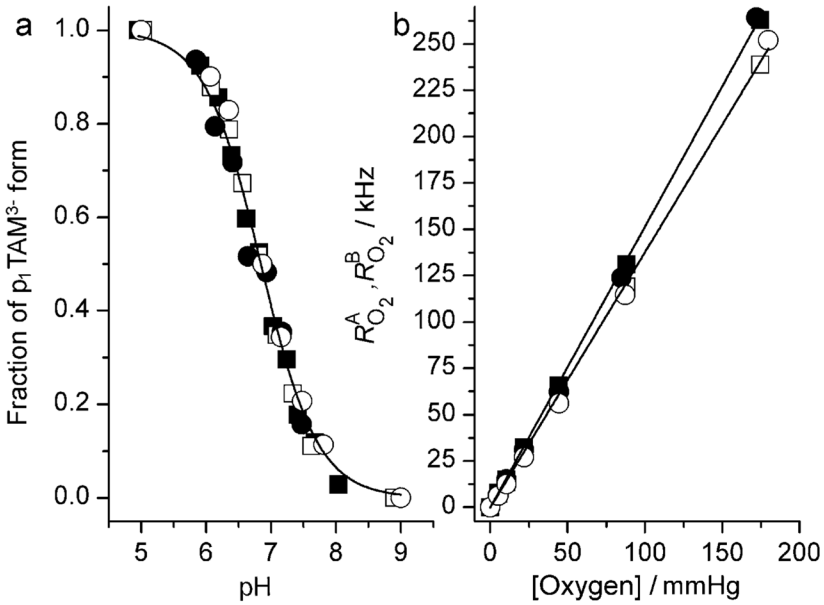

Figure 3.

a) Dependency of the fraction p_A of the p_1TAM^{3-} form on the pH calculated from FT-EPR spectra measured in Na-phosphate buffer, 150 mM NaCl, at different buffer concentrations: 0 (○), 1 (●), 2 (■), and 5 mM (□). Solid lines represent the best fit by a conventional titration curve yielding identical values of pK_a^2 =(6.85 ± 0.05). b) The dependency of oxygen-induced relaxation rates, $R_{O2}{}^A$ (filled symbols) and $R_{O2}{}^b$ (open symbols), on the oxygen partial pressure calculated from FT-EPR spectra acquired at pH 4.5, pH 10 (circles), and pH 6.9 (squares). Lines represent the best linear fits yielding the values of the bimolecular rate constants, $k_{O2}{}^A$ =1.51 kHzmmHg^{-1} and $k_{O2}{}^B$ =1.38 kHzmmHg^{-1}.

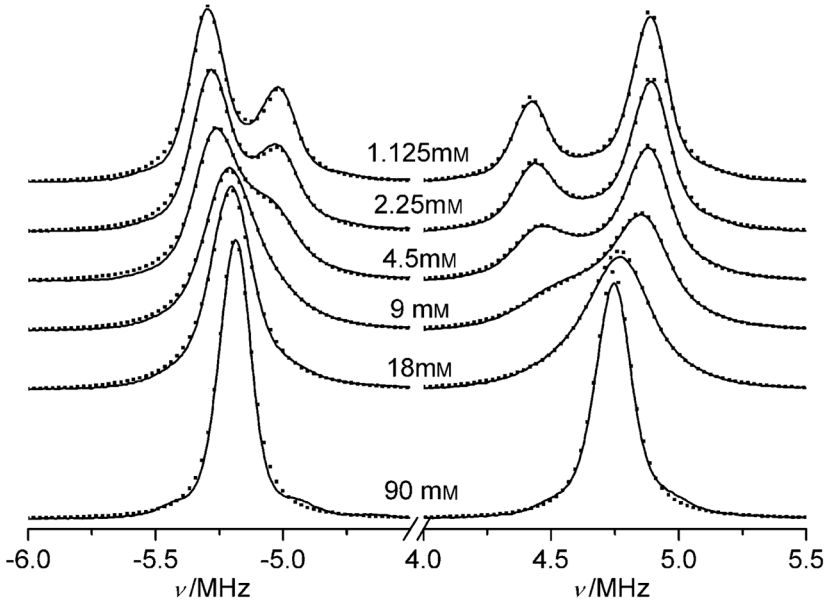

Figure 4.

FT-EPR spectra of 0.2 mM p_1TAM measured in 150 mM NaCl aqueous solutions at different Na-phosphate buffer concentrations, pH 6.53. The dotted lines are calculated spectra.

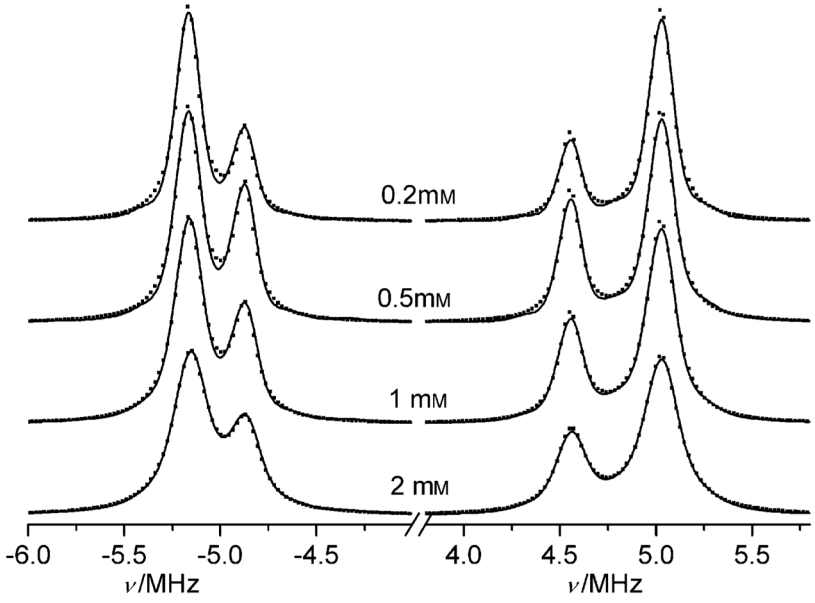

Figure 5.

FT-EPR spectra of various concentrations of p_1TAM (indicated near the spectra) in anoxic 150 mM NaCl solutions in the absence of phosphate buffer. The dotted lines are calculated spectra.

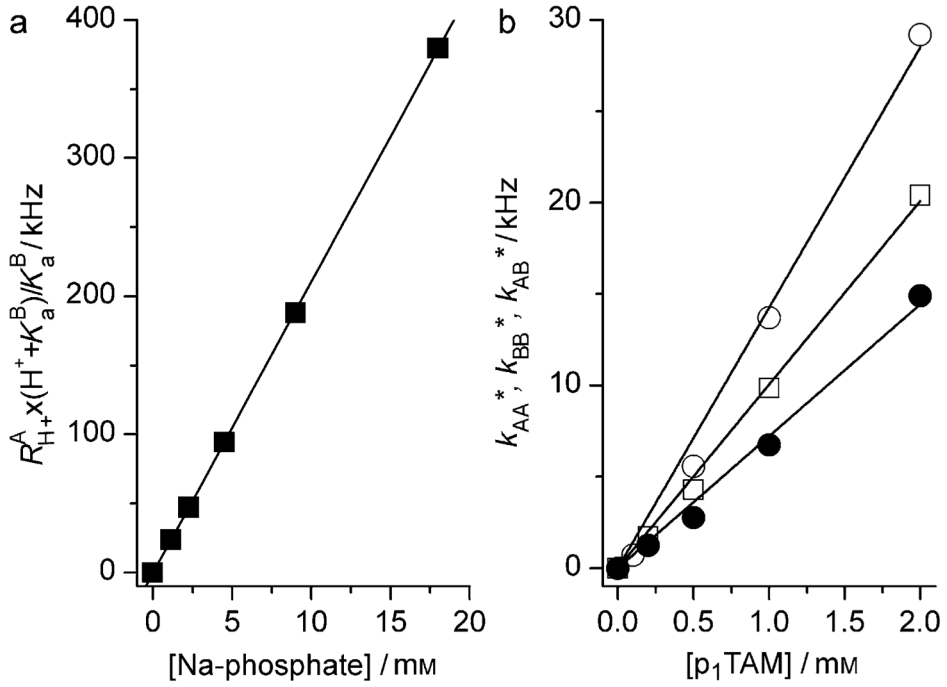

Figure 6.

a) Dependency of the term $R^{A}_{H+} \times (K_a^B + H^+)/K_a^B$ on the concentration of the Na-phosphate buffer obtained by fitting the EPR spectra shown in Figure 4. The solid line represents a linear fit yielding the value of k_f = 21 kHzmM $^{-1}$. b) The dependency of the observed rates of spin self-exchange, k_{AA}* (○), k_{BB}* (●), and k_{AB}* (□) on the concentration of the p_1TAM probe. Solid lines represent linear fits yielding the values of bimolecular rate constants, k_{AA} = 14.3 kHzmM^{-1}, k_{BB} = 7.2 kHzmM^{-1}, and k_{AB} = 10 kHzmM^{-1}.

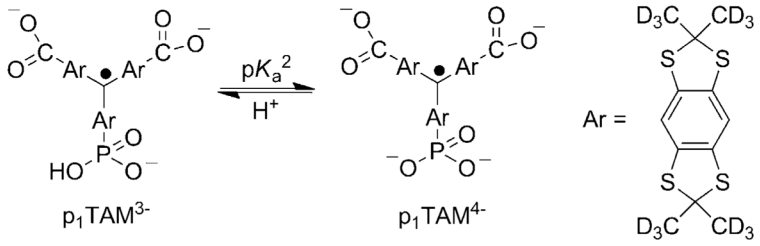

Scheme 1.

The acid–base equilibrium for the monophosphonated trityl radical, p_1TAM (pK_a^2 = 6.9). The pK_a^1 value for the first dissociation of the phosphono group is about 1.3 and the pK_a value for the dissociation of the carboxy groups is about 2.6.[8]

Table 1

Relaxation times of the p_1TAM probe.

	pH 10[a]	**pH 10**[b]	**pH 4.5**[a]	**pH 4.5**[b]
T_1 [μs]	21 ± 1	0.57 ± 0.05	18 ± 1	0.62 ± 0.05
T_2 [μs]	11 ± 1	0.54 ± 0.05	6.0 ± 0.5	0.61 ± 0.05

[a] Measured in anoxic solution of 0.2 mM p_1TAM;

[b] Measured in ambient air.

Table 2

The values of pH, pO_2, [Pi], and [p_1TAM] calculated from FT-EPR spectra measured in p_1TAM solutions of different compositions.

pH, ± 0.03		pO_2 [mmHg], ± 1 mmHg		[Pi] [mM], ± 0.1 mM		[p_1TAM] [mM], ± 0.1 mM	
Prep.	**Calc.**	**Prep.**	**Calc.**	**Prep.**	**Calc.**	**Prep.**	**Calc.**
7.40	7.42	10	9	0.05	0.1	0.05	0.0
7.10	7.07	13	14	0.5	0.4	0.5	0.6
7.00	7.02	6	6	0.5	0.4	0.5	0.6
6.95	6.93	0	1	0.5	0.4	0.5	0.6
6.50	6.54	0	−1	4.5	4.5	0.2	0.2
6.50	6.45	0	0	0	0	2.0	2.0